

# Transmission phase of a quantum dot and statistical fluctuations of partial-width amplitudes

Rodolfo A. Jalabert,<sup>1</sup> Guillaume Weick,<sup>1</sup> Hans A. Weidenmüller,<sup>2</sup> and Dietmar Weinmann<sup>1</sup>

<sup>1</sup>*Institut de Physique et Chimie des Matériaux de Strasbourg,  
Université de Strasbourg, CNRS UMR 7504, F-67034 Strasbourg, France*

<sup>2</sup>*Max-Planck-Institut für Kernphysik, D-69029 Heidelberg, Germany*

Experimentally, the phase of the amplitude for electron transmission through a quantum dot (transmission phase) shows the same pattern between consecutive resonances. Such universal behavior, found for long sequences of resonances, is caused by correlations of the signs of the partial-width amplitudes of the resonances. We investigate the stability of these correlations in terms of a statistical model. For a classically chaotic dot, the resonance eigenfunctions are assumed to be Gaussian distributed. Under this hypothesis, statistical fluctuations are found to reduce the tendency towards universal phase evolution. Long sequences of resonances with universal behavior only persist in the semiclassical limit of very large electron numbers in the dot and for specific energy intervals. Numerical calculations qualitatively agree with the statistical model but quantitatively are closer to universality.

PACS numbers: 05.45.Mt, 03.65.Vf, 03.65.Nk, 73.23.-b

## I. INTRODUCTION

The phase of the transmission amplitude (in short: the transmission phase) is a key element in the description of coherent transport of electrons through a quantum dot (QD). The phase is not accessible via standard conductance measurements [1–3]. A breakthrough was achieved with the advent of phase-sensitive experiments on ballistic two-dimensional QDs in the Coulomb-blockade regime [4]. The QD was placed in one arm of a phase-coherent ring. The Aharonov-Bohm conductance oscillations measured as a function of the magnetic flux piercing the ring in an open (or “leaky”) interferometer [5] yielded an indirect determination of the transmission phase of the QD.

Variation of the plunger gate voltage (and, thereby, of the electrostatic potential) on the QD made it possible to investigate sequences of resonances. Long sequences of in-phase resonances were observed [5] in relatively large QDs (with around 200 electrons on the dot) suggesting *universal* behavior. In very small QDs (with up to 14 electrons) the relative phase of consecutive resonances appeared to be random [6]. That case was dubbed the “mesoscopic regime” (even though both cases are in the regime of coherent transport which is usually referred to as the mesoscopic regime).

Electron transport through a QD connected to two single-mode leads as depicted in Fig. 1 can be viewed as a quantum scattering process. According to the Friedel sum rule, the scattering phase shift increases by  $\pi$  when the electrochemical potential  $\mu = E_F + V_g$  is swept through a resonance by changing the electrostatic potential  $V_g$  on the dot. Here,  $E_F$  is the Fermi energy in the leads. The transmission phase follows the scattering phase shift unless the transmission amplitude has a zero [7–9]. In that case, the crossing of the origin of the complex plane produces a phase slip of  $\pi$ . The experimentally observed phase locking of resonances in large QDs then necessitates a phase slip of  $\pi$  or equivalently, a zero of the transmission amplitude between every pair of resonances. In the literature that situation is indistinctly referred to as phase locking, phase slip or transmission zero between consecutive resonances.

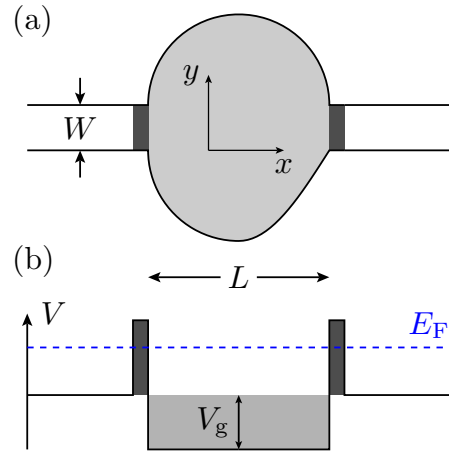


FIG. 1. (Color online) (a) Sketch of an asymmetric quantum dot (light gray) connected to leads through tunnel barriers (dark gray). (b) Cut of the potential landscape in the longitudinal direction. A nearby plunger gate allows to change the electrostatic potential  $V_g$  within the dot. The Fermi level (blue dashed line) determines the wavenumbers  $k_F$  in the leads and  $k$  in the dot, through  $E_F = \hbar^2 k_F^2 / 2m = \hbar^2 k^2 / 2m - V_g$ .

The observed phase locking has posed a theoretical puzzle since it appears to contradict the expectation that eigenstates of different resonances are uncorrelated. Numerous theoretical papers have addressed the emergence of universal behavior in large QDs [1–3, 7–17]. Some works have pointed to the importance of electronic correlations in establishing universal behavior [15], while detailed many-body numerical calculations recently disputed such a view [17]. Other works described the Coulomb blockade on the QD in terms of the constant-interaction model, reducing the problem to a single-particle one [9–13, 16]. The universality of the transmission phase is then related to the existence of broad levels generated by charging effects [12–14] and/or to properties of the single-particle wavefunctions representing the resonances [9–11, 16]. In particular, it was proposed in Ref. [16] that quantum chaos on the QD causes spatial correlations of the single-

particle wavefunctions and, thus, is at the root of the experimentally observed emergence of universality.

In the present paper we critically examine the proposal of Ref. [16]. Assuming a Gaussian distribution for the single-particle eigenfunctions of the QD, we calculate the statistical fluctuations of the lead-dot coupling amplitudes and determine the probability of zeros of the transmission amplitude. We show that the fluctuations weaken the tendency towards universality found in Ref. [16].

The behavior of the transmission phase is determined by the partial-width amplitudes (PWAs) of the resonances in the QD. With consecutive resonances labeled by a running index  $n$ , the left (right) PWA of the  $n^{\text{th}}$  resonance with eigenfunction  $\psi_n(x, y)$  reads [18]

$$\gamma_n^{l(r)} = \sqrt{\frac{\hbar^2 k_F P_c}{m}} \int_0^W dy \psi_n(x^{l(r)}, y) \Phi_{l(r)}(y). \quad (1)$$

Within the constant-interaction model and under neglect of the magnetic field in the QD,  $\psi_n(x, y)$  can be chosen real. The geometry is sketched in Fig. 1(a). The leads of width  $W$  are connected to the QD by tunnel barriers of transparency  $P_c$ . The distance between entrance and exit leads is  $L \gg W$ . The first transversal subband wavefunction in the left (right) lead is written as  $\Phi_{l(r)}$ , and the integration in Eq. (1) is along the transverse coordinate  $y$  at the entrance (exit) of the QD located at  $x = x^{l(r)}$ . The Fermi wavenumber in the leads is denoted by  $k_F$ , and the effective electron mass by  $m$ .

We consider the generic case (referred to as *restricted off-resonance* behavior [17]) where the PWAs do not fluctuate strongly with  $n$ . Then the behavior of the transmission amplitude is determined by the PWAs of the two resonances closest in energy. The transmission amplitude vanishes between the  $n^{\text{th}}$  and  $(n+1)^{\text{st}}$  resonance if and only if [9]

$$D_n = \gamma_n^l \gamma_n^r \gamma_{n+1}^l \gamma_{n+1}^r > 0. \quad (2)$$

Then there is an overall phase slip of  $\pi$  between the two resonances. We mention in passing that there are cases where the PWAs fluctuate strongly (*unrestricted off-resonance* behavior) and where the criterion (2) does not apply [17].

## II. GAUSSIAN DISTRIBUTION OF PARTIAL-WIDTH AMPLITUDES

Actual values of the PWAs depend on the geometry of the QD. A generic description can only be based upon a statistical approach. In this framework the probability  $\mathcal{P}(D_n < 0)$  for condition (2) to be violated has been calculated in various scenarios (i.e., disordered QDs [9] and ballistic chaotic quantum billiards [16]). We follow that line using a particular statistical hypothesis related to quantum chaos, and we discuss various parameter regimes.

We define the parity of the  $n^{\text{th}}$  resonance as the sign of  $\gamma_n^l \gamma_n^r$  and the probability of having a positive parity as  $\mathcal{P}(\gamma_n^l \gamma_n^r > 0)$ . Under the assumption that the eigenfunctions of the  $n^{\text{th}}$

and  $(n+1)^{\text{st}}$  resonances are statistically uncorrelated, we have

$$\begin{aligned} \mathcal{P}(D_n < 0) &= \mathcal{P}(\gamma_n^l \gamma_n^r > 0) [1 - \mathcal{P}(\gamma_{n+1}^l \gamma_{n+1}^r > 0)] \\ &\quad + \mathcal{P}(\gamma_{n+1}^l \gamma_{n+1}^r > 0) [1 - \mathcal{P}(\gamma_n^l \gamma_n^r > 0)]. \end{aligned} \quad (3)$$

We assume that the classical dynamics of electrons moving independently in the QD is chaotic. In this case, according to the Voros-Berry conjecture, the Wigner function is ergodically distributed on the energy manifold of phase space [19–21]. This assumption implies that the eigenfunction  $\psi_n$  belonging to the eigenvalue  $\epsilon_n = \hbar^2 k_n^2 / 2m$  has a Gaussian probability density  $p(\psi_n)$  [22]. For a two-dimensional billiard with area  $\mathcal{A}$  and position vector  $\mathbf{r} = (x, y)$ , the probability density is given by

$$p(\psi_n) = \mathcal{N} \exp \left( -\frac{1}{2} \int_{\mathcal{A}} d\mathbf{r} \int_{\mathcal{A}} d\mathbf{r}' \psi_n(\mathbf{r}) K(\mathbf{r}, \mathbf{r}'; k_n) \psi_n(\mathbf{r}') \right) \quad (4)$$

where  $\mathcal{N}$  is the normalization constant. The function  $K$  is defined by

$$\int_{\mathcal{A}} d\mathbf{r} K(\mathbf{r}, \mathbf{r}'; k) J_0(k|\mathbf{r} - \mathbf{r}'|) = \mathcal{A} \delta(\mathbf{r} - \mathbf{r}'), \quad (5)$$

where  $J_0$  is the zeroth Bessel function of the first kind. Equation (4) implies  $\langle \psi_n \rangle = 0$  and a correlation of the values of the eigenfunction  $\psi_n$  at two points  $\mathbf{r}$  and  $\mathbf{r}'$  given by [20]

$$\langle \psi_n(\mathbf{r}) \psi_n(\mathbf{r}') \rangle = \frac{1}{\mathcal{A}} J_0(k_n |\mathbf{r} - \mathbf{r}'|). \quad (6)$$

The angular brackets denote the average over  $p(\psi_n)$ . The eigenfunctions belonging to different resonances are uncorrelated, so that  $p(\psi_1, \psi_2, \dots) = \prod_n p(\psi_n)$ .

We recall that the spatial correlation of wavefunctions has also been derived from information theory [23] or, in the case of weakly disordered systems, with the aid of supersymmetry techniques [24, 25]. The effects of spectral, position, and directional averages in expression (6) have been thoroughly discussed in Refs. [26] and [27]. Furthermore, this important relation has been experimentally tested in the eigenmodes of resonant microwave cavities [28] and numerically checked in different dynamical systems [29–32], especially in the context of the so-called rate of quantum ergodicity (i.e., the rate in which the quantum-mechanical expectation value tends to its mean value upon approaching the semiclassical limit of large energies). Along these lines, Srednicki and Stiernelof [33] used the Gaussian hypothesis (4) to show that the root-mean-square amplitude of the statistical fluctuations around the mean value given by Eq. (6) decrease in the semiclassical limit as  $(k^2 \mathcal{A}_R)^{-1/4}$ , where  $\mathcal{A}_R$  is the area of the billiard used for a spatial average of the autocorrelator ( $\mathcal{A}_R \ll \mathcal{A}$ ).

According to Eqs. (1) and (4), each PWA is the sum of Gaussian-distributed amplitudes and, hence, has a Gaussian distribution, too. From  $\langle \psi_n \rangle = 0$  and  $\langle \psi_n \psi_{n'} \rangle = 0$  for  $n \neq n'$  we have  $\langle \gamma_n^{l(r)} \rangle = 0$  and  $\langle \gamma_n^{l(r)} \gamma_{n'}^{l(r)} \rangle = 0$  for  $n \neq n'$ . For each  $n$  the distribution of the PWAs is then characterized by

the three second moments  $\langle \gamma_n^l \gamma_n^l \rangle$ ,  $\langle \gamma_n^r \gamma_n^r \rangle$ , and  $\langle \gamma_n^l \gamma_n^r \rangle$ . Left-right symmetry of the couplings between the leads and the QD implies the equality

$$\sigma_n^2 = \langle \gamma_n^l \gamma_n^l \rangle = \langle \gamma_n^r \gamma_n^r \rangle. \quad (7)$$

With

$$\rho_n = \frac{1}{\sigma_n^2} \langle \gamma_n^l \gamma_n^r \rangle, \quad (8)$$

the joint probability density of the left and right PWA is

$$p(\gamma_n^l, \gamma_n^r) = \frac{1}{2\pi\sigma_n^2\sqrt{1-\rho_n^2}} \times \exp\left(-\frac{(\gamma_n^l)^2 + (\gamma_n^r)^2 - 2\rho_n\gamma_n^l\gamma_n^r}{2\sigma_n^2(1-\rho_n^2)}\right). \quad (9)$$

The probability for the product  $\gamma_n^l\gamma_n^r$  to be positive is obtained from Eq. (9) as

$$\mathcal{P}(\gamma_n^l\gamma_n^r > 0) = \frac{1}{2} + \frac{1}{\pi} \arcsin(\rho_n). \quad (10)$$

Completely correlated (anti-correlated) PWAs corresponding to  $\rho_n = 1$  ( $-1$ ) lead to  $\mathcal{P}(\gamma_n^l\gamma_n^r > 0) = 1$  ( $0$ , respectively), while in the uncorrelated case we have  $\rho_n = 0$  and  $\mathcal{P}(\gamma_n^l\gamma_n^r > 0) = 1/2$ .

For the evaluation of Eq. (3) we have to determine the dependence of  $\rho_n$  on  $k_n$ . With the QD being chaotic, the distribution of spacings  $\epsilon_n - \epsilon_{n+1}$  of nearest eigenvalues is given by the Wigner surmise. However,  $\rho_n$  is expected to be a smooth function of  $k_n$  on the scale of the mean wavenumber difference  $\Delta k_n = \pi/k_n L^2$ . Therefore,

$$\mathcal{P}(D_n < 0) \simeq 2f(k_n) + \Delta k_n f'(k_n) \quad (11)$$

with

$$f(k) = \frac{1}{4} - \frac{1}{\pi^2} \arcsin^2(\rho(k)). \quad (12)$$

The extreme values of  $\rho$  are  $\rho = \pm 1$ . Therefore,  $d\rho/dk = 0$  for  $|\rho| = 1$ , and the expression (11) is well defined for all values of  $\rho$ .

Equation (11) shows that there are two possible reasons for violations of the universal behavior  $\mathcal{P}(D_n < 0) = 0$ . (i) The condition  $|\rho| = 1$  may be violated so that  $\gamma_n^l$  and  $\gamma_n^r$  are not perfectly correlated or anticorrelated, and  $f(k_n) \neq 0$ . (ii) Even if the previous condition is met,  $\Delta k_n$  may not be negligible. Reason (i) becomes the dominant one in the semiclassical regime [16], where  $\Delta k_n \propto 1/k_n L^2$ , or when the spectral average over the resonances is taken. We return to that point in Sec. IV.

### III. SECOND MOMENTS OF PARTIAL-WIDTH AMPLITUDES

We use Eqs. (1) and (6) to calculate  $\sigma_n^2$  and  $\rho_n$  as defined in Eqs. (7) and (8). We assume that QD and leads have hard

walls. The first transversal subband wavefunction for the left (right) lead then reads

$$\Phi_{1(r)}(y) = \sqrt{\frac{2}{W}} \sin\left(\frac{\pi y}{W}\right), \quad (13)$$

and we have

$$\begin{aligned} \sigma_n^2 &= \alpha \int_0^W dy \int_0^W dy' \langle \psi_n(x^1, y) \psi_n(x^1, y') \rangle \\ &\times \left[ \cos\left(\frac{\pi}{W}(y' - y)\right) - \cos\left(\frac{\pi}{W}(y' + y)\right) \right] \\ &= \frac{2\alpha W^2}{\mathcal{A}} \int_0^1 dz J_0(k_n W z) \\ &\times \left[ (1 - z) \cos(\pi z) + \frac{1}{\pi} \sin(\pi z) \right], \end{aligned} \quad (14)$$

where  $\alpha = \hbar^2 k_F P_c / mW$ . We have introduced dimensionless integration variables, changed to their difference  $z$  and half their sum, and integrated over the latter variable. For  $k_n W \ll 1$  we approximate the argument of  $J_0$  in Eq. (14) by unity, obtaining

$$\sigma_n^2 \simeq \frac{\alpha W^2}{\mathcal{A}} \frac{8}{\pi^2}, \quad (15)$$

while for  $k_n W \gg 1$  the integral over  $z$  is strongly suppressed because of the oscillating character of  $J_0$ . We show in the Appendix that

$$\sigma_n^2 \simeq \frac{\alpha W^2}{\mathcal{A}} \frac{2}{k_n W}. \quad (16)$$

For the correlator  $\langle \gamma_n^l \gamma_n^r \rangle$  we obtain analogously

$$\begin{aligned} \langle \gamma_n^l \gamma_n^r \rangle &= \frac{2\alpha W^2}{\mathcal{A}} \int_0^1 dz J_0\left(k_n L \sqrt{1 + (W/L)^2 z^2}\right) \\ &\times \left[ (1 - z) \cos(\pi z) + \frac{1}{\pi} \sin(\pi z) \right]. \end{aligned} \quad (17)$$

Analytical results for  $\langle \gamma_n^l \gamma_n^r \rangle$  are obtained in the following regimes. For  $k_n W \ll L/W$  we have

$$\langle \gamma_n^l \gamma_n^r \rangle \simeq \frac{\alpha W^2}{\mathcal{A}} \frac{8}{\pi^2} J_0(k_n L), \quad (18)$$

while for  $k_n W \gg L/W \gg 1$  we show in the Appendix that

$$\langle \gamma_n^l \gamma_n^r \rangle \simeq \frac{\alpha W^2}{\mathcal{A}} \frac{2}{k_n W} \cos(k_n L). \quad (19)$$

The corresponding results for the correlator  $\rho$  are obtained by combining the results (15) and (16) with Eqs. (18) and (19). The value of  $k_n$  defines three regimes that are depicted in Fig. 2(a) for the case  $L/W = 5$ . These are

- (i) the one-mode regime  $1 < k_n L < L/W$  (red dashed line), where

$$\rho_n \simeq J_0(k_n L); \quad (20)$$

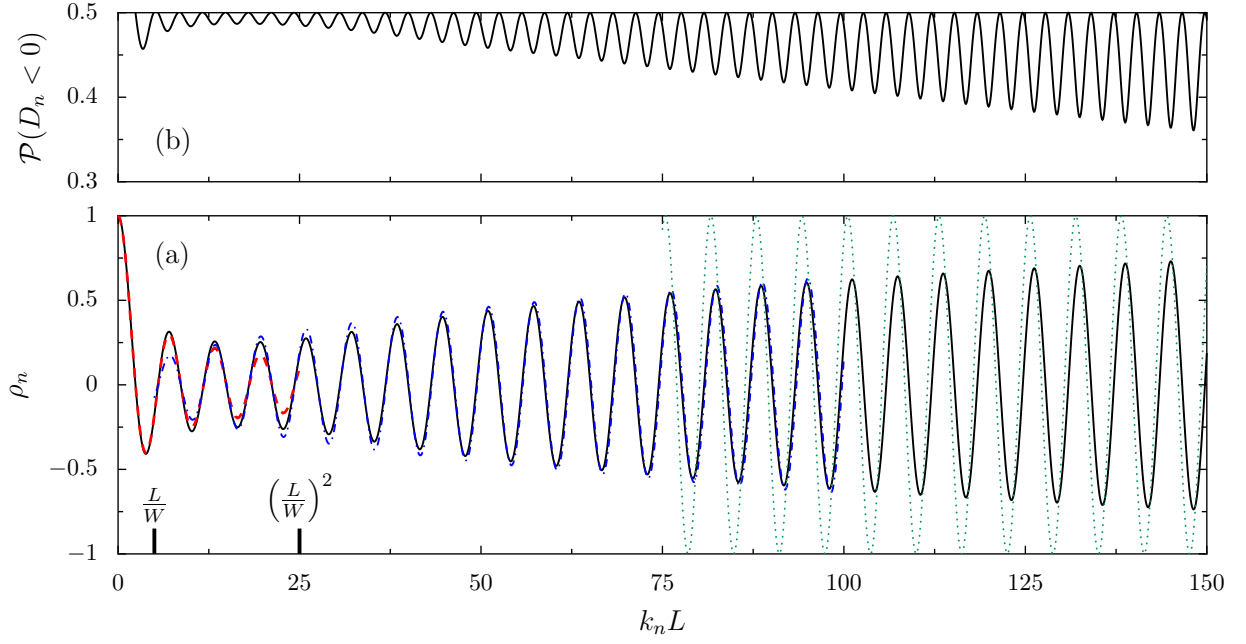


FIG. 2. (Color online) (a) The correlator  $\rho_n$  defined in Eq. (8), calculated numerically from the integrals in Eqs. (14) and (17), is plotted as a function of  $k_n L$  for  $L/W = 5$  (black solid line). The dashed red line represents the approximate result of Eq. (20) valid for  $k_n L \lesssim L/W$ . The dash-dotted blue line represents the result of Eq. (21) for the intermediate regime, and the green dotted line gives the semiclassical result of Eq. (22). (b) The probability  $\mathcal{P}(D_n < 0)$  as a function of  $k_n L$ , calculated from Eqs. (11) and (12) and the numerical result for  $\rho_n$ .

- (ii) the intermediate regime  $L/W < k_n L < (L/W)^2$  (blue dash-dotted line), where

$$\rho_n \simeq \frac{4}{\pi^2} k_n W J_0(k_n L); \quad (21)$$

- (iii) the semiclassical regime  $k_n L \gg (L/W)^2$  (green dotted line), where

$$\rho_n \simeq \cos(k_n L). \quad (22)$$

In addition, the value of  $\rho_n$  obtained by numerical evaluation of Eqs. (14) and (17) is shown as a black line in Fig. 2(a). The oscillation of  $\rho_n$  around zero is due to the Bessel function in the integrand of Eq. (17). The amplitude approaches unity in the semiclassical regime ( $k_n L \gg 1$ ). Figure 2(b) shows the resulting probability  $\mathcal{P}(D_n < 0)$  calculated from  $\rho_n$  using Eqs. (11) and (12). For the parameters chosen, the contribution of the second term on the right-hand side of Eq. (11) is significant only for  $k_n L \lesssim 10$ . Therefore, the deviation of  $\mathcal{P}(D_n < 0)$  from zero is almost exclusively due to the lack of perfect correlation between the PWAs belonging to neighboring resonances.

We recall that the condition for adjacent resonances to cause with probability 1 a lapse in the phase of the transmission amplitude is given by  $\mathcal{P}(D_n < 0) = 0$ . According to Eqs. (11) and (22) this condition is met only in the semiclassical limit for distinct values of  $k$  for which

$$\mathcal{P}(D_n < 0) \simeq \frac{1}{2} - 2 \left( \left\{ \frac{k_n L}{\pi} \right\} - \frac{1}{2} \right)^2. \quad (23)$$

Here  $\{x\}$  denotes the fractional part of  $x$ . Extrapolation of the data shown in Fig. 2(b) to larger values of  $k_n L$  suggests that  $k$  intervals which meet that condition do indeed exist.

#### IV. ENSEMBLE AVERAGE VERSUS SPECTRAL AVERAGE — NUMERICAL RESULTS

The results in Sec. III and in Fig. 2 represent averages over the Gaussian ensemble defined in Sec. II. How are we to relate these averages with actual data obtained by measurements of a single QD (and not on an ensemble of QDs)? The answer would be simple if  $\mathcal{P}(D_n < 0)$  were independent of  $k$  as we could then employ the usual ergodicity argument and equate the ensemble average obtained in the statistical approach with the running average of data over  $k$ . However, the oscillations of  $\mathcal{P}(D_n < 0)$  away from the completely uncorrelated value  $1/2$  towards smaller values shown in Fig. 2(b) increase as we approach the semiclassical limit  $k_n L \rightarrow \infty$ . Therefore, the actual value of  $\mathcal{P}(D_n < 0)$  becomes increasingly dependent on  $k$ , and the relation between the two averages acquires crucial importance.

First, we may think of the correlator in Eq. (6) as being the result of an averaging process performed on the actual eigenfunction of the  $n^{\text{th}}$  resonance for fixed distance  $|\mathbf{r} - \mathbf{r}'|$ . Such spatial averaging, when performed over a domain larger than the de Broglie wavelength, improves the rate of quantum ergodicity [32, 33] by suppressing the fluctuations around the mean value of the wavefunction product under consideration. The integrals over  $y$  and  $y'$  in the defining Eq. (14) for  $\sigma_n^2$  and in the corresponding expression for  $\langle \gamma_n^1 \gamma_n^x \rangle$  partly amount to



such an average.

This argument is purely *ad hoc*, however. Moreover, it does not resolve the issue of the dependence of  $\mathcal{P}(D_n < 0)$  on  $k$ . The actual value of  $k$  in the experiments is not known. To make up for that, an average of  $\mathcal{P}(D_n < 0)$  over one period in  $k_n L$  was considered in Ref. [16]. Under that proposal, the second term on the right-hand side of Eq. (11) yields in the semiclassical limit a negligible contribution since  $f$  becomes a periodic function of  $k$ . Using Eq. (23), the first term yields  $1/3$  on average, rendering the occurrence of long sequences of in-phase resonances quite unlikely. However, averaging over an entire period in  $k_n L$  is not necessary. Indeed, equality of ensemble average and running average is guaranteed provided the latter extends over a sufficiently large set of resonances. The average spacing  $\Delta k_n = \pi/k_n L^2$  of resonances becoming very small in the semiclassical limit, it suffices to consider an averaging interval much smaller than a full period in  $k_n L$  to obtain a meaningful average. Since the last term on the right-hand side of Eq. (11) is semiclassically negligible, long sequences of in-phase resonances do exist for  $k$  values where  $|\rho|$  is close to unity and  $\mathcal{P}(D_n < 0)$  is close to zero. The length of such sequences of in-phase resonances decreases as  $\mathcal{P}(D_n < 0)$  deviates from zero.

In Ref. [16], numerical calculations done for the configuration of Fig. 1 versus plunger gate voltage yielded for large values of  $kL$  long sequences of in-phase resonances. The difference between the number of resonances and the number of transmission zeros in a given  $k$ -interval was found to become progressively small in the semiclassical limit. Here we report on a more systematic numerical study. We calculate the distribution of  $D_n$  [cf. Eq. (2)] and compare that with the probability  $\mathcal{P}(D_n < 0)$  predicted by the Gaussian hypothesis [Eqs. (11) and (12)].

When the plunger gate voltage  $V_g$  is varied over a sufficiently large interval, the  $k$  dependence of the complex transmission amplitude  $t$  displays a sequence of peaks. Figure 3 shows an example of such a sequence, whose length corresponds to changing  $kL$  by about  $3\pi$ . Figure 3(a) presents the peaks of the absolute value of  $t(k)$ , and Fig. 3(b) shows that  $t$  approximately follows circles in the complex plane, indicating that most of the peaks have Breit-Wigner form. At the  $n^{\text{th}}$  resonance we accordingly use

$$t(k) = \sum_n \frac{\gamma_n^l \gamma_n^r}{\epsilon(k) - \epsilon_n + i\Gamma_n/2} \quad (24)$$

with  $\Gamma_n = |\gamma_n^l|^2 + |\gamma_n^r|^2$  to extract the product  $\gamma_n^l \gamma_n^r$  and to obtain  $D_n$ .

In the complex plane of Fig. 3(b) we can easily recognize the relatively broad peaks, represented by a dense set of points along a circle, representing data for increasing values of  $kL$ , while the very sharp ones correspond to only a few points on the chosen  $kL$  grid. When there is a transmission zero between two peaks,  $t$  continues to turn anticlockwise in the same half-plane. If there is a finite minimal value of  $|t|$  between two peaks, a switch of half-plane occurs before turning (also counter-clockwise) for the  $kL$  values corresponding to the second peak. The tendency towards universality is already

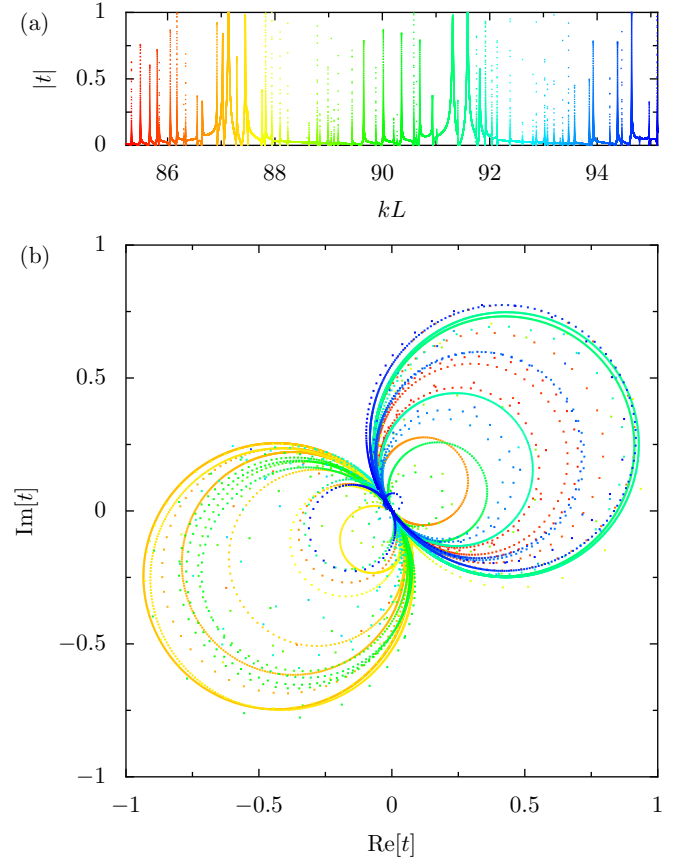


FIG. 3. (Color online) (a) Absolute value of the transmission amplitude  $t$  for the setup in Fig. 1, as a function of  $kL$ . (b) The transmission amplitude presented in the complex plane, for the same values of  $kL$  (which are encoded by the color of the data points).

noticeable in this restricted sequence of peaks for a single stadium. Peaks of similar color (close in  $k_n L$ ) tend to stay in one of the half-planes, but there are occasional switches between the two half-planes.

To determine the distribution of  $D_n$  with sufficiently good statistics, we have taken two steps. First, we have combined a sequence of  $D_n$  values within some  $k_n$  interval much larger than the level spacing. Second, we have combined data generated from stadia with different shapes. We describe these steps in turn. For fixed stadium shape, the length  $\delta/L$  of the sampling interval is bounded from above by the fact that according to Fig. 2(b) the distribution of  $D_n$  is expected to be an oscillatory function of  $k$ . Values of  $\delta \approx \pi$  would mix different distribution patterns. On the other hand, values of  $\delta \ll \pi$  reduce the number of resonances in the interval and increase the statistical error. We have chosen  $\delta = \pi/4$ . We have improved the local statistics by combining data from six successive  $k_n$  intervals given by  $[k_n + j\pi/L, k_n + j\pi/L + \delta]$  with  $j = -3, -2, -1, 0, 1, 2$ . Since the smooth oscillations of  $\mathcal{P}(D_n < 0)$  are expected to be quasi-periodic with period  $\pi/L$ , that procedure should not cause any problems. We have used that procedure for a total of fifteen different stadium shapes. Fourteen of these were generated from Fig. 1(a)

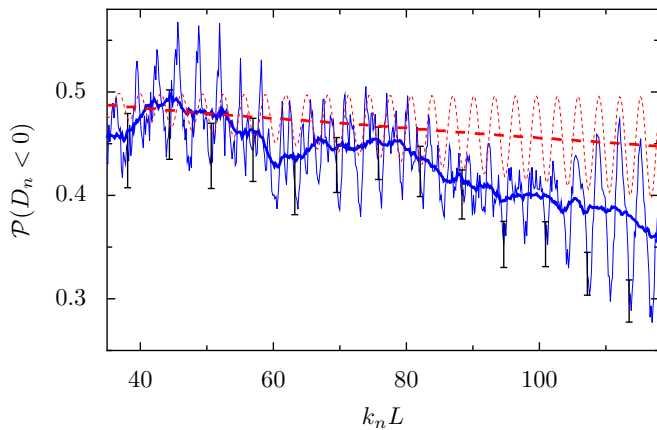


FIG. 4. (Color online) Blue solid lines: numerically obtained  $\mathcal{P}(D_n < 0)$  (see text) using a smoothing  $k_n$  interval of  $\delta/L$  with  $\delta = \pi/4$  and  $\pi$  (thin and thick lines, respectively). The error bars of some of the data points for the smaller smoothing interval indicate the statistical error. Red dashed lines:  $\mathcal{P}(D_n < 0)$  from the statistical model, Eqs. (11) and (12), using smoothing intervals with  $\delta = \pi/4$  and  $\pi$  (thin and thick lines, respectively).

by deforming different quarter circles of the stadium. Each shape yielded a sequence of peaks that was uncorrelated from the others [34].

Figure 4 shows  $\mathcal{P}(D_n < 0)$  obtained numerically as described above (thin blue solid line), together with the analytic result of Eqs. (11) and (12), locally averaged over  $k_n$  intervals of length  $\delta/L$  with  $\delta = \pi/4$  (thin red dashed line). The thin red dashed line is a smoothed version of the solid line in Fig. 2(b). The difference between the two curves is very small. We have assigned statistical error bars to some points of the numerically generated  $\mathcal{P}(D_n < 0)$ . Consistently with our previous analysis we find for the lowest part of the interval shown that the statistical errors are quite significant, while for larger values of  $k_n$  we can be confident that the features observed in the curve  $\mathcal{P}(D_n < 0)$  are statistically robust. For instance, the  $\pi/L$  quasi-periodicity of  $\mathcal{P}(D_n < 0)$  is clearly seen in the thin blue solid curve of Fig. 4.

Figure 4 shows that for  $k_n L \gtrsim 60$  the numerically generated values of  $\mathcal{P}(D_n < 0)$  are systematically smaller than those of the statistical model. This is displayed very clearly by the two thick solid blue and dashed red lines obtained by averaging the data in  $k_n$ -intervals of length  $\pi/L$ . We recall that the statistical model yields a saturation value of  $1/3$  only in the semiclassical limit while the numerical results attain that value already for  $k_n L \simeq 120$ . The early approach of the numerical results to the universality condition  $\mathcal{P}(D_n < 0) = 0$  predicted semiclassically may have important consequences in the analysis of the experiments and for wavefunction correlations.

The surprising quantitative discrepancy between our numerical results and the predictions of the statistical model may be due to several assumptions of the latter model that may not fully apply. Firstly, there is a correction to Eq. (6) that is due to classical trajectories [35]. This correction is significant when the two arguments of the wavefunction correlator are widely

separated. In principle the correction could be taken into account within a semiclassical numerical approach. Secondly, Eq. (6) does not account for boundary effects. The boundary conditions for the resonance wavefunctions are of mixed Dirichlet-Neumann type (vanishing  $\psi_n$  along the hard walls of the billiard and vanishing normal derivative at the points connecting the dot to the leads). The ensuing corrections could in principle be calculated following the prescription of Ref. [36]. Thirdly, the Gaussian hypothesis is perhaps not appropriate to describe the higher moments of the wavefunction distribution, since it is based on an ergodic distribution on the energy shell. Such an assumption has its limitations since it has been shown that, in a two-dimensional phase-space, a delta-function on the energy shell cannot represent a positive operator in the Weyl representation [37]. That is, a delta-function cannot be a true Wigner function. This result has been recently generalized [38] to any curved surface of dimension  $2d - 1$  in a phase-space of dimension  $2d$ . We have not investigated any of these challenging issues yet.

## V. CONCLUSIONS

Leaky Aharonov-Bohm interferometers have given access to the transmission phase of a quantum dot placed in one of the arms of the interferometer. Long sequences of in-phase resonances observed experimentally pose a theoretical puzzle. Assuming that the Coulomb blockade in the dot can be treated within the constant-interaction model, we have reduced the theoretical calculation of the transmission phase to a one-body problem. The phase evolution between neighboring resonances is determined by their parities. For each resonance the parity is defined as the sign of the product of the partial-width amplitudes for entrance and exit leads and is determined directly by the resonance eigenfunction. This chain of thought has led us from a flagship problem in mesoscopic physics to one of the fundamental issues of quantum chaos, that is, the statistical properties of wavefunctions of a system which is classically chaotic.

Assuming a Gaussian distribution for the eigenfunctions of a classically chaotic dot, we have calculated the probability of having in-phase resonances. We have done so for different regimes defined by the ratio of the de Broglie wavelength  $1/k$  in the dot and the length scales of the problem (the width  $W$  of the leads and the distance  $L$  between the entrance and exit leads). We found that the fluctuations of the partial width amplitudes are relevant. Complete in-phase behavior of the resonances is obtained only in the semiclassical limit of large  $kL$ . Even in this regime, in-phase behavior is not universal but occurs only within certain energy intervals. Numerical calculations yield qualitatively the same behavior. However, with increasing  $kL$  the numerical results tend to be systematically smaller than predicted by the statistical model and, thus, closer to universal behavior.

We stress that the present attempt to explain the experimental results of Refs. [4, 5] within the statistical model or our numerical calculations is in line with much work in mesoscopic physics. The constant-interaction model is used to reduce the

physics to that of a single-particle problem. The statistical model further assumes that the chaotic nature of the single-particle classical dynamics in the quantum dot justifies the use of the Voros-Berry conjecture and random-matrix theory. It is important to recall that such an approach has led to a successful description of the statistical distribution of the height of the Coulomb blockade peaks [39–41]. Moreover, the long-range (in energy) modulation of the peak-height distribution found in some of the experiments (not accounted for in the simplest random-matrix description) is found [42] to be due to spatial correlations of the resonance wavefunctions described by Eq. (6).

It is tempting to think of improvements of the numerical calculations that might lead to a better agreement with the experimental data. A more realistic model of the quantum dot could be helpful in yielding information concerning the regime in which the dot operates (see Sec. III). Such calculations would encounter a number of difficulties, however. Neither the precise form of the self-consistent single-particle confinement potential of the dot nor its modification due to a change of the plunger voltage are known. It seems likely that the actual situation is quite different from that sketched in Fig. 1 where a change of  $V_g$  merely shifts the floor of the potential. In fact, a deformation of the confinement potential caused by changing the plunger voltage has been held responsible for the phase locking of consecutive resonances [10] and for the energy modulation of the peak-height distribution [43]. In work using density-functional theory to calculate the electronic structure of lithographically defined quantum dots [44] it was found that some properties (like the peak-height distribution) are relatively robust with respect to details of the confining potential, while others (like the energy modulation of the peak heights) are not. Still we believe that more realistic models for quantum dots, together with the study of wavefunction fluctuations beyond the Gaussian assumption, appear as promising avenues opened by the present investigation.

#### ACKNOWLEDGMENTS

We thank A. M. Ozorio de Almeida for helpful discussions and for letting us know unpublished results [38], and R. A. Molina for useful remarks on the manuscript. We acknowledge the financial support from the ANR through grant ANR-08-BLAN-0030-02.

#### APPENDIX: APPROXIMATE INTEGRATIONS IN THE SEMICLASSICAL LIMIT

We evaluate Eqs. (14) and (17) in the semiclassical limit. Introducing the variable  $x = k_n W z$ , we write Eq. (14) as

$$\sigma_n^2 = \frac{2\alpha W^2}{\mathcal{A}} \frac{1}{k_n W} \int_0^{k_n W} dx J_0(x) \times \left[ \left(1 - \frac{x}{k_n W}\right) \cos\left(\frac{\pi x}{k_n W}\right) + \frac{1}{\pi} \sin\left(\frac{\pi x}{k_n W}\right) \right]. \quad (25)$$

In the first and third terms on the right-hand side of Eq. (25) we use  $k_n W \gg 1$  to extend the upper integration limits for these highly oscillating integrands to infinity. We use

$$\int_0^\infty dx J_0(x) \cos\left(\frac{\pi x}{k_n W}\right) = \frac{1}{\sqrt{1 - (\pi/k_n W)^2}}, \quad (26)$$

$$\int_0^\infty dx J_0(x) \sin\left(\frac{\pi x}{k_n W}\right) = 0. \quad (27)$$

The second term on the right-hand side of Eq. (25) can be integrated by parts. Using that

$$\int dx J_0(x) x = J_1(x) x, \quad (28)$$

with  $J_1$  the first Bessel function of the first kind, we get

$$\int_0^{k_n W} dx J_0(x) x \cos\left(\frac{\pi x}{k_n W}\right) = \frac{-J_1(k_n W)}{1 - (\pi/k_n W)^2}. \quad (29)$$

Combining Eqs. (25)–(27) and (29), we obtain expression (16) as the leading-order term in an expansion in powers of  $(k_n W)^{-1}$ .

In Eq. (17) we use  $L \gg W$ , the semiclassical limit  $k_n W^2/L \gg 1$ , and the asymptotic expansion of the Bessel function to obtain the leading-order term

$$\langle \gamma_n^l \gamma_n^r \rangle = \frac{2\alpha W^2}{\mathcal{A}} \int_0^1 dz \sqrt{\frac{2}{\pi \theta(z)}} \cos\left(\theta(z) - \frac{\pi}{4}\right) \times \left[ (1 - z) \cos(\pi z) + \frac{1}{\pi} \sin(\pi z) \right], \quad (30)$$

where  $\theta(z) = k_n L + (k_n W^2/2L)z^2$ . Using the same inequalities we evaluate the integral by the stationary-phase method. The stationary point is at  $\bar{z} = 0$ , and we have

$$\langle \gamma_n^l \gamma_n^r \rangle \simeq \frac{2\alpha W^2}{\mathcal{A}} \sqrt{\frac{2}{\pi k_n L}} \int_0^\infty dz \cos\left(\theta(z) - \frac{\pi}{4}\right). \quad (31)$$

The evaluation of this Fresnel integral yields Eq. (19).

- 
- [1] G. Hackenbroich, *Phys. Rep.* **343**, 463 (2001).
  - [2] A. Levy Yeyati and M. Büttiker, *Phys. Rev. B* **52**, R14360 (1995).
  - [3] A. Aharony, O. Entin-Wohlman, B. I. Halperin, and Y. Imry, *Phys. Rev. B* **66**, 115311 (2002).
  - [4] A. Yacoby, M. Heiblum, D. Mahalu, and H. Shtrikman, *Phys. Rev. Lett.* **74**, 4047 (1995).
  - [5] R. Schuster, E. Buks, M. Heiblum, D. Mahalu, V. Umansky, and H. Shtrikman, *Nature* **385**, 417 (1997).
  - [6] M. Avinun-Kalish, M. Heiblum, O. Zarchin, D. Mahalu, and V. Umansky, *Nature* **436**, 529 (2005).
  - [7] H.-W. Lee, *Phys. Rev. Lett.* **82**, 2358 (1999).
  - [8] T. Taniguchi and M. Büttiker, *Phys. Rev. B* **60**, 13814 (1999).
  - [9] A. Levy Yeyati and M. Büttiker, *Phys. Rev. B* **62**, 7307 (2000).
  - [10] G. Hackenbroich, W. D. Heiss, and H. A. Weidenmüller, *Phys. Rev. Lett.* **79**, 127 (1997).
  - [11] R. Baltin, Y. Gefen, G. Hackenbroich, and H. A. Weidenmüller, *Eur. Phys. J. B* **10**, 119 (1999).
  - [12] R. Baltin and Y. Gefen, *Phys. Rev. Lett.* **83**, 5094 (1999).
  - [13] P. G. Silvestrov and Y. Imry, *Phys. Rev. Lett.* **85**, 2565 (2000).
  - [14] S. Kim and H.-W. Lee, *Phys. Rev. B* **73**, 205319 (2006).
  - [15] C. Karrasch, T. Hecht, A. Weichselbaum, Y. Oreg, J. von Delft, and V. Meden, *Phys. Rev. Lett.* **98**, 186802 (2007).
  - [16] R. A. Molina, R. A. Jalabert, D. Weinmann, and P. Jacquod, *Phys. Rev. Lett.* **108**, 076803 (2012).
  - [17] R. A. Molina, P. Schmitteckert, D. Weinmann, R. A. Jalabert, and P. Jacquod, *Phys. Rev. B* **88**, 045419 (2013).
  - [18] Y. Alhassid, *Rev. Mod. Phys.* **72**, 895 (2000).
  - [19] A. Voros, *Ann. Inst. Henri Poincaré, Sect. A* **24**, 31 (1976).
  - [20] M. V. Berry, *J. Phys. A: Math. Gen.* **10**, 2083 (1977).
  - [21] Notice that the ergodicity of eigenfunctions in quantum graphs has also been recently considered in S. Gnutzmann, J. P. Keating, and F. Piotet, *Phys. Rev. Lett.* **101**, 264102 (2008), and *Ann. Phys. (N.Y.)* **325**, 2595 (2010).
  - [22] M. Srednicki, *Phys. Rev. E* **54**, 954 (1996).
  - [23] C. Jarzynski, *Phys. Rev. E* **56**, 2254 (1997).
  - [24] V. N. Prigodin, N. Taniguchi, A. Kudrolli, V. Kidambi, and S. Sridhar, *Phys. Rev. Lett.* **75**, 2392 (1995).
  - [25] I. V. Gornyi and A. D. Mirlin, *Phys. Rev. E* **65**, 025202 (2002).
  - [26] F. Toscano and C. H. Lewenkopf, *Phys. Rev. E* **65**, 036201 (2002).
  - [27] B. Li and D. C. Rouben, *J. Phys. A: Math. Gen.* **34**, 7381 (2001).
  - [28] B. Eckhardt, U. Dörr, U. Kuhl, and H.-J. Stöckmann, *Europhys. Lett.* **46**, 134 (1999).
  - [29] R. Aurich and F. Steiner, *Physica D* **64**, 185 (1993).
  - [30] B. Li and M. Robnik, *J. Phys. A: Math. Gen.* **27**, 5509 (1994).
  - [31] A. Bäcker, R. Schubert, and P. Stifter, *Phys. Rev. E* **57**, 5425 (1998).
  - [32] A. Bäcker and R. Schubert, *J. Phys. A: Math. Gen.* **35**, 539 (2002).
  - [33] M. Srednicki and F. Stiernelof, *J. Phys. A: Math. Gen.* **29**, 5817 (1996).
  - [34] Each individual sequence for a given geometry exhibits the quasi-periodicity of  $\pi/L$  in its  $k_n$ -dependence of the partial distribution of  $\mathcal{P}(D_n < 0)$ , but with an arbitrary phase-shift. In order to compare equivalent behaviors of  $\mathcal{P}(D_n < 0)$  for a given  $k_n$ , we adjusted a rigid shift for each geometry (for the whole  $V_g$  interval) by minimizing its departure from the analytic curve of the statistical model.
  - [35] S. Hortikar and M. Srednicki, *Phys. Rev. Lett.* **80**, 1646 (1998).
  - [36] J. D. Urbina and K. Richter, *Phys. Rev. E* **70**, 015201 (2004).
  - [37] N. L. Balazs, *Physica A* **102**, 236 (1980).
  - [38] A. M. Ozorio de Almeida, *arXiv:1403.2261 [quant-ph]* (2014).
  - [39] R. A. Jalabert, A. D. Stone, and Y. Alhassid, *Phys. Rev. Lett.* **68**, 3468 (1992).
  - [40] A. M. Chang, H. U. Baranger, L. N. Pfeiffer, K. W. West, and T. Y. Chang, *Phys. Rev. Lett.* **76**, 1695 (1996).
  - [41] J. A. Folk, S. R. Patel, S. F. Godijn, A. G. Huibers, S. M. Cronenwett, C. M. Marcus, K. Campman, and A. C. Gossard, *Phys. Rev. Lett.* **76**, 1699 (1996).
  - [42] E. E. Narimanov, H. U. Baranger, N. R. Cerruti, and S. Tomsovic, *Phys. Rev. B* **64**, 235329 (2001).
  - [43] R. O. Vallejos, C. H. Lewenkopf, and E. R. Mucciolo, *Phys. Rev. B* **60**, 13682 (1999).
  - [44] M. Stopa, *Phys. Rev. B* **54**, 13767 (1996).